# Experimental study of MMI structures in a switchable continuous-wave thulium-doped all-fiber laser

A. CAMARILLO-AVILÉS,[1] M. V. HERNÁNDEZ-ARRIAGA,[2] R. LÓPEZ-ESTOPIER,[1,3] M. BELLO-JIMÉNEZ[1*], O. POTTIEZ,[4] M. DURÁN-SÁNCHEZ,[3,5] B. IBARRA-ESCAMILLA,[5] and M. V. ANDRÉS[6]

*[1]Instituto de Investigación en Comunicación Óptica, Universidad Autónoma de San Luis Potosí, Av. Karakorum No. 1470 Lomas 4ª Secc., 78210, San Luis Potosí, Mexico*
*[2]Unidad Académica Multidisciplinaria Zona Media, Universidad Autónoma de San Luis Potosí, Carr. Rioverde-San Ciro Km. 4, Col. Puente del Carmen, 79615 Rioverde, San Luis Potosí, México*
*[3]Consejo Nacional de Ciencia y Tecnología (CONACYT), Av. Insurgentes Sur No. 1582, Col. Crédito Constructor, Del. Benito Juárez, México, 039040, Ciudad de México*
*[4]Centro de Investigaciones en Óptica (CIO), Loma del Bosque No. 115, Col. Lomas del Campestre, 37150 León, Guanajuato, Mexico*
*[5]Instituto Nacional de Astrofísica, Óptica y Electrónica (INAOE), Luis Enrique Erro No. 1, Departamento de Óptica, 72000 Puebla, Mexico*
*[6]Universidad de Valencia, Departamento de Física Aplicada y Electromagnetismo, ICMUV, c/Dr. Moliner 50, Burjassot, 46100 Valencia, Spain.*
*[*]miguel.bello@uaslp.mx*

**Abstract:** Switchable multi-wavelength laser emission from a thulium-doped all-fiber laser is reported by implementing a tapered and a non-tapered multi-modal interference (MMI) filters. The MMI structure relies on a coreless optical fiber spliced in between two single-mode optical fibers. For the non-tapered case, a minimum insertion loss of 12.60 dB is achieved around the 2-μm region, from which stable generation of commutable dual-wavelength emission at 1986.34 nm and 2017.38 nm is obtained. On the other hand, the tapered MMI structure performs a minimum insertion loss of 8.74 dB at the 2-micron region, allowing a stable triple-wavelength emission at 1995.4 nm, 2013.3 nm, and 2038.3 nm. In addition, commutable dual-wavelength emission was also obtained at 1997.9 nm and 2032.1 nm. The generated laser lines perform bandwidths of around 50 pm, low peak spectral power fluctuations and signal-to-noise ratio of 50 dB.

## 1. Introduction

Thulium-doped all-fiber lasers operating in the continuous-wave (CW) regime have attracted a great deal of attention in the last years due to their large number of applications in many research fields and practical areas. A few examples of these applications are related to the development of supercontinuum light sources [1-3], telecommunications [4,5], gas sensing [6,7], medical procedures [8-11], high power laser sources [12-14], among others. In the last decade, different configurations of all-fiber lasers have been demonstrated to perform high-quality CW and multi-line emissions in the 2 μm spectral region [15-28]. In those approaches, interferometric solutions possess important advantages such as low-insertion loss, robustness, compact size, and simplicity in fabrication [19-23], allowing precise control of laser emission and providing narrow linewidth generation, fine-tuning range, and a high degree of repeatability. However, in most of the above-mentioned approaches, the schemes are optimized for the thulium band and performs laser emission that usually extends from 1700 to 2000 nm, but rarely exceed the 2-micron wavelength limit. Therefore, the development of new interferometric all-fiber devices performing laser operation beyond 2000 nm is an issue of growing research interest.

In recent years, many efforts have been accomplished to develop multi-mode interference (MMI) devices in thulium-doped fiber lasers (TDFLs), and a small number of MMI filtering devices have been proposed and demonstrated [29]. By using this type of fiber-optic device, multi-wavelength operation was successfully achieved in the thulium band region [30-33]. Now, with the purpose of demonstrating its versatility, a tapered and non-tapered MMI fiber structure is analyzed as a wavelength-selective filter to achieve 2-μm wavelength

emission. This work, to the best of our knowledge, presents the first approach demonstrating stable multi-wavelength generation in the 2-μm band by using this type of interferometric device.

In this manuscript, the MMI effect in both a tapered and a non-tapered fiber structures that implement a multi-mode optical fiber is analyzed. The MMI filter relies on a coreless optical fiber (COF) spliced in between two single-mode fibers (SMFs), forming a SMF-COF-SMF structure. The filter is suspended in air and fixed at one end to a linear translation stage to induce bending after displacement. Initial experiments were performed with a non-tapered MMI filter, achieving commutable dual-wavelength operation with a narrow bandwidth of ~50 pm, signal-to-noise ratio (SNR) over 50 dB, and maximum output power of 13.35 mW. For the tapered case, laser operation at single-, dual-, and triple-wavelength emission is obtained with characteristics of narrow linewidth (50 pm) and high SNR (~60 dB), with many of its laser lines centered beyond the 2000 nm. Compared with recently reported TDFLs schemes that include a MMI filter, our proposal is easy reproducible. It preserves the simplicity and robustness of all-fiber arrangements and could be considered a reliable fiber-optic device that provides a high degree of repeatability.

## 2. Experimental setup

A schematic view of the experimental setup is shown in Fig. 1. The fiber laser consists of a ring cavity with total length of 22.81 m. The scheme utilizes a 6-m long double-clad thulium-doped fiber (TDF, Coractive DCF-TM-10-128) as the gain medium, which in turn is pumped through a (2+1)×1 multimode pump combiner (Lightcomm C170115271). Following a counterclockwise direction, an in-line polarization controller (PC) is included to adjust the intracavity polarization state before the MMI spectral filter. Next, a fiber isolator is incorporated to force unidirectional light propagation, and the cavity is closed by splicing a 75/25 fiber coupler to the thulium fiber. The laser output is obtained from the 25% port of the fiber coupler. For proper adjustment of the PC and appropriate control of the MMI filter spectral response, stable multi-wavelength CW emission is achieved beyond 2000 nm.

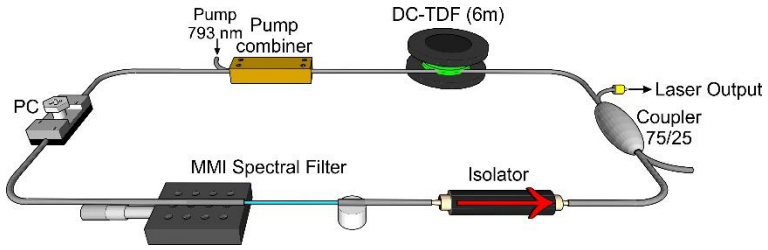


Fig. 1. Schematic of MMI thulium-doped all-fiber laser.

Laser emission was analyzed using an optical spectrum analyzer (OSA, Yokogawa AQ6375 with 50 pm resolution) and the output power monitored with a thermal detector (ThorLabs S303C). All the elements that compose the laser system are commercially accessible and available, no special fiber optic components were added in this setup.

## 3. The MMI filter

The spectral filter is composed of a short section of COF (Thorlabs, FG125A) spliced in between two single mode optical fibers, as shown in Fig. 2. The COF performs a similar behavior to that of a multi-mode optical fiber with step-index profile when the surrounding refractive index is lower than the silica rod. Therefore, the filter arrangement is easily implemented in air. Its operation principle relies on the self-imaging effect caused by the MMI phenomenon along the coreless fiber. In this manner, the excitation and interference of high-order modes depends on the diameter and length of the COF segment. A theoretical estimation of the peak wavelength response as a function of the diameter and length of the MMI filter is obtained from the following equation [34]:

$$\lambda_0 = (p\, n_{MMF}\, D^2_{MMF}) / L, \text{ with } p = 0, 1, 2, \ldots$$

where $n_{MMF}$, $D_{MMF}$ and $L$ are the refractive index, diameter, and length of the multi-mode fiber (MMF), respectively, while $p$ is the self-image number. A precise length of the COF segment is crucial for an optimal wavelength filter design. Our setup is designed to operate with the fourth self-image number, where it was found that insertion loss was lower and wavelength bandwidth narrower compared to the other image numbers, i.e., $p$ = 0, 1, 2 or 3 [35].

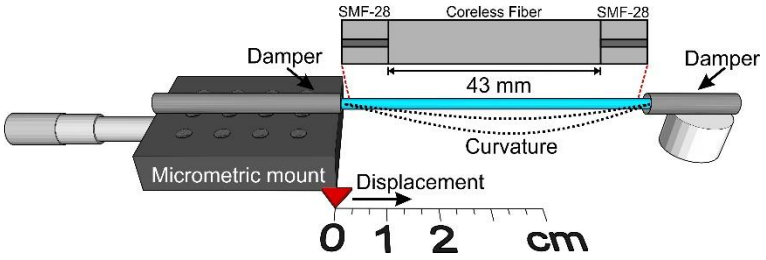


Fig. 2. Structure of the SM-COF-SM spectral filter

The filter structure is composed of a COF segment of 43 mm in length which is spliced in between two SMF-28 fibers sections. One SMF-28 fiber end is positioned over a standard micrometric mount with 0.01 mm resolution and 25.4 mm of maximum displacement, while the other fiber end is fixed to an aluminum base to support the filter in air. The arrangement provides bending and easy control of the filter after displacement, see the schematic view of the filter depicted in Fig. 2. The moving end is displaced along the horizontal plane to produce a controlled bending of the coreless fiber that leads to a blue shift response of the peak wavelength transmission of the MMI filter. The characterization of the MMI filter was performed with a fiber-based supercontinuum light source covering a wavelength range from 1860 to 2200 nm [3] and the transmittance spectrum was measured as the ratio between the output and the input optical spectra. Fig. 3(a) shows the transmittance spectrum corresponding to 1 mm of displacement of the translation stage. At this position, up to five resonances are observed and the minimum insertion loss is reached in the 2-micron region. The transmittance spectrum displays peak resonances at 1960.5 nm, 2007.8 nm, 2032.0 nm, 2078.2 nm and 2106.2 nm, respectively (see markers in Fig. 3(a)), exhibiting insertion losses ranging between 17 and 7 dB. Fig. 3(b) shows the evolution of the peak resonance (PR) wavelengths in function of the linear stage displacement. As it can be observed, the tracked peaks undergo a blue shift as the linear translation stage is displaced from 0 to 2.5 mm in steps of 0.05 mm.

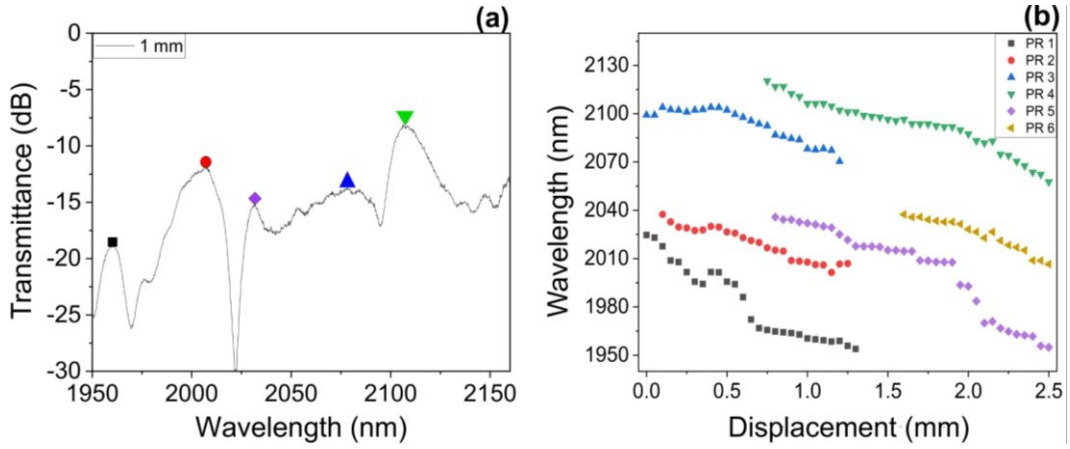


Fig.3 (a) Transmittance spectrum of the MMI filter for 1 mm linear stage displacement. (b) Evolution of the tracked resonances as a function of the displacement of the linear stage.

## 4. Experimental results and discussion

### *4.1 The non-tapered MMI filter*

The MMI filter in the laser setup allows the generation of dual-wavelength emissions, which are controlled by the gradual adjustment of the micrometric mount displacement, enabling an extra degree of flexibility to manipulate the output power and allow wavelength regulation. Characteristics of the dual-wavelength laser operation are illustrated in Fig. 4. A comparative view of the MMI filter transmittance (red line) when applying a 0.70 mm displacement of the micrometric mount and of the corresponding lasing lines (black line) is provided in Fig. 4(a) at the pump power of 4.45 W. Under these conditions, dual-wavelength operation with channel spacing (Δλ) of 31.04 nm was observed, the laser lines are located at 1986.34 nm and 2017.38 nm with maximum peak spectral powers of −17.65 and −22.87 dBm, respectively. The stability of the laser operation was characterized by performing peak spectral power and wavelength measurement of each lasing line at time intervals of 5 minutes over a 60-minute observation period, as shown in Fig. 4(b). The maximum wavelength fluctuation was ±150 pm, whereas the maximum output power variation was measured as ±1.59 dBm. The spectral evolution is depicted in the Fig. 4(c), where no significant fluctuations are observed. A close-up view of the 1986.49 nm laser line is provided in Fig. 4(d), where a signal-to-noise ratio (SNR) of 53.43 dB is observed together with a −3 dB bandwidth of ~60 pm. The output spectrum shown in Fig. 4(e) depicts the laser emission at 2017.38 nm, from which a SNR of 46.78 dB and −3-dB bandwidth of ~50 pm is observed.

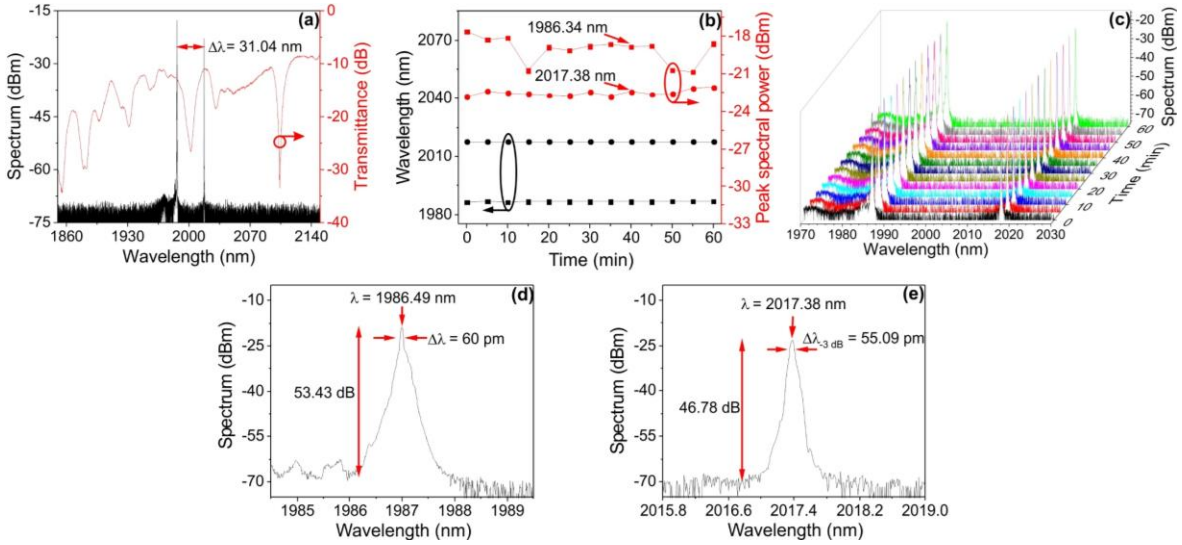


Fig. 4. Characteristics of the dual-wavelength emission by displacing the micrometric mount at 0.70 mm and setting the pump power at 4.45 W. (a) Dual-wavelength emission (black line) and MMI filter transmittance (red line). (b) Stability of dual-wavelength emission over a 60-minute observation time. (c) Spectral evolution. Close-up view of the generated laser lines at (d) 1986.49 nm and (e) 2017.38 nm.

The scheme also allows switchable single-wavelength operation of the dual-wavelength TDFL by adjusting the PC. To analyze the switching process, the displacement of the micrometric mount and the pump power level were maintained fixed throughout the experiments. Thus, the switching process consists of conserving only one of the two laser lines, either at 1986.34 nm or 2017.38 nm. By carefully adjusting the pressure and rotation of the PC, the setup allows switching from dual- to single-wavelength operation. Fig. 5(a) shows the single-wavelength operation at 2017.43 nm with a peak spectral power of −18.35 dBm. A measurement of the laser efficiency was obtained from the linear relation between the output and pump powers. From the inset shown in Fig. 5(a), a laser efficiency of 0.28 % was measured. The stability was also characterized over 60 minutes of time span with measurement intervals of 5 min. Fig. 5(b) shows the laser fluctuations in peak spectral power, output power and wavelength shifting, the maximum fluctuations were measured as ±1.16 dBm, ±0.04 mW, and ±413 pm, respectively. The spectral evolution is shown in the Fig. 5(c). In a similar manner, it was possible to switch to the other emission wavelength, see Fig. 5(d). A slight adjustment of the PC was necessary, however, since there is no well-defined MMI transmission peak at this wavelength, and lasing takes place in the proximity

of the transmission peak. This is a very common behavior in multi-wavelength fiber lasers [36]. For these adjustments, the single-emission wavelength was centered at 1988 nm with a maximum output peak spectral power of −17.24 dBm. As can be observed, there exists a redshift in wavelength of 1.67 nm with respect to the corresponding line in dual-wavelength operation, this shift was possibly caused by temperature variations surrounding the experimental setup, originating a redistribution of the output power along its corresponding maximum peak transmittance. The efficiency of this single-wavelength laser was measured as 0.30 %, as depicted in the inset. Fig. 5(e) shows the laser stability recorded over 60 minutes at intervals of 5 minutes. Maximum fluctuations of peak spectral power, output power and wavelength were measured as ±0.76 dBm, ±0.09 mW, and ±6 pm, respectively. The spectral evolution of the single laser emission is shown in the Fig. 5(f).

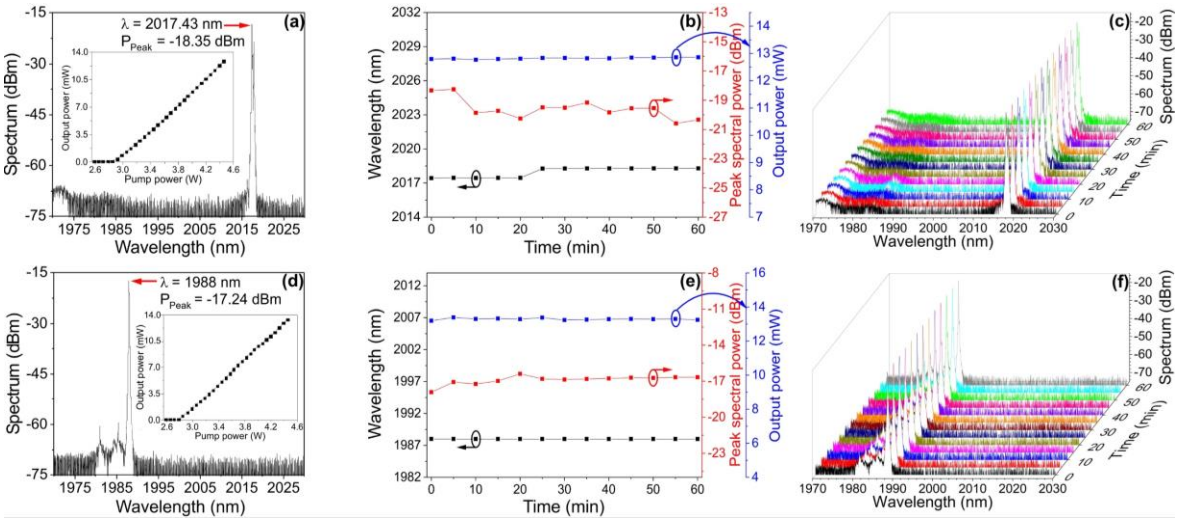


Fig. 5. Switching behavior of the dual-wavelength emission. Single-wavelength operation at (a) 2017.43 nm and (d) 1988.0 nm. The inset includes the output power versus pump power. Laser stabilities for (b)-(c) 2017.43 nm and (e)-(f) 1988.0 nm wavelengths recorded over a time span of 60 minutes.

From the results presented above, we conclude that the proposed approach based on a non-tapered MMI filter structure demonstrates stable operation in both single- and dual-wavelength laser operations, allowing the independent switching of each laser line by rotating the polarization controller. Compared with recently reported TDFLs based on MMI, our scheme achieves laser emission at the 2-micron band, demonstrating the potential of MMI filters based on conventional fibers to perform laser emission beyond this wavelength limit. As the next step, with the objective of improving the characteristics of laser emission, a MMI structure based on a tapered fiber is described in the next section.

### *4.2 The tapered MMI filter*

A schematic view of the tapered MMI filter structure is illustrated in Fig. 6(a). To fabricate this device, a SMF-28 fiber was initially tapered down to 80 µm in diameter and then cleaved at the middle of its waist, as a result two tapered fiber ends were obtained. Subsequently, a uniformly tapered segment of coreless optical fiber was sandwiched between the tapered ends of the SMF-28 fibers. The tapering process was performed using a standard fusion and pulling technique [37], in which an oscillating flame composed of a controlled mixture of oxygen and butane was employed to fabricate a biconical tapered fiber. The MMI structure includes two transition sections of SMF-28 fiber at both ends of the structure, exhibiting a long exponentially decaying transition profile. The tapered COF has a length of 18 mm and maintains a uniform diameter of 80 µm. Similarly to the non-tapered case, the length of the COF is determinant for the peak wavelength response, as discussed in

[38]. The insertion loss for the tapered MMI filter was measured as 8.74 dB at 2000 nm. The transmission spectrum of the filter was estimated in a similar manner as the non-tapered filter, but in this case the displacement of the filter was set at its initial position, i.e., 0 mm, the corresponding spectrum is observed in Fig. 6(b). The output spectrum shows six maxima transmission peaks within the measured spectral window ranging from 1850 to 2150 nm. Compared with the non-tapered case, this structure yields substantial improvements in terms of insertion losses, which now range between 9 and 3 dB. This improvement is attributed to the reduction in length of the coreless fiber, which is reduced by a factor of ~2.4 for the tapered case.

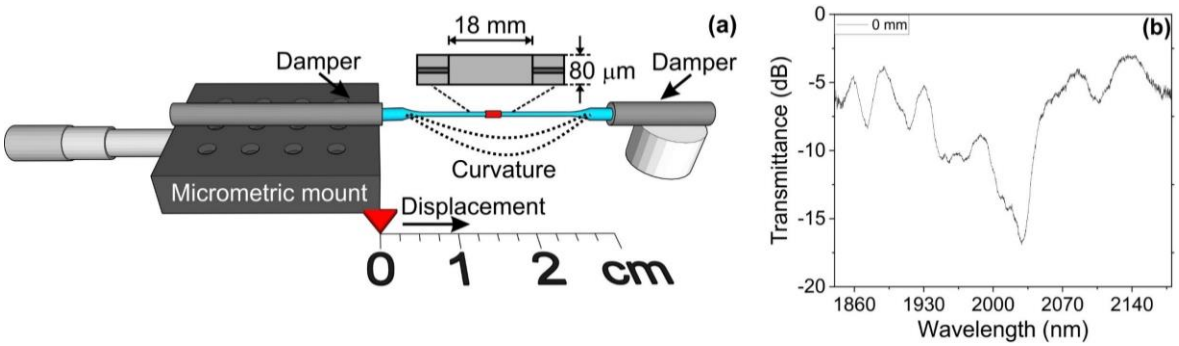


Fig. 6. (a) Structure of the tapered MMI spectral filter. (b) Spectral response of the filter at its initial position.

### *4.2.1 Switching behavior and triple-wavelength operation*

Substituting the non-tapered MMI filter by the tapered one into the laser cavity offers important improvements. One of them is the possibility to operate in a triple-wavelength emission in the 2-μm band. The triple-wavelength operation was obtained when the tapered MMI filter was bent with a displacement of 3.2 mm and the pump power was increased to 4.87 W. The rotation of the PC was necessary to equilibrate gain and losses between the lasing lines. Fig. 7(a) shows the output spectra obtained by increasing the pump power in a range between 2.90 and 4.87 W. It can be observed that laser emission is initially achieved at 2013.27 nm with a pump power of 2.90 W. Then, dual-wavelength operation starts at 3.92 W pump power, with an additional lasing mode appearing at 1995.41 nm, on the left of the original lasing mode. The triple-wavelength operation is reached at 4.87 W pump power, corresponding to simultaneous laser emissions at 1995.41 nm, 2013.27 nm and 2038.32 nm. A comparative view of the MMI filter transmittance (red line) and the triple-wavelength emission (black line) is shown in Fig. 7(b), where a wavelength spacing of ~21.45 nm between adjacent lines is measured. Close-up views of the emitted laser lines are provided in Figs. 7(c)–(e). The maximum SNR observed is estimated as 58.05 dB for the central wavelength. Moreover, this emission demonstrates narrow linewidths for all laser lines, with values around 50 pm.

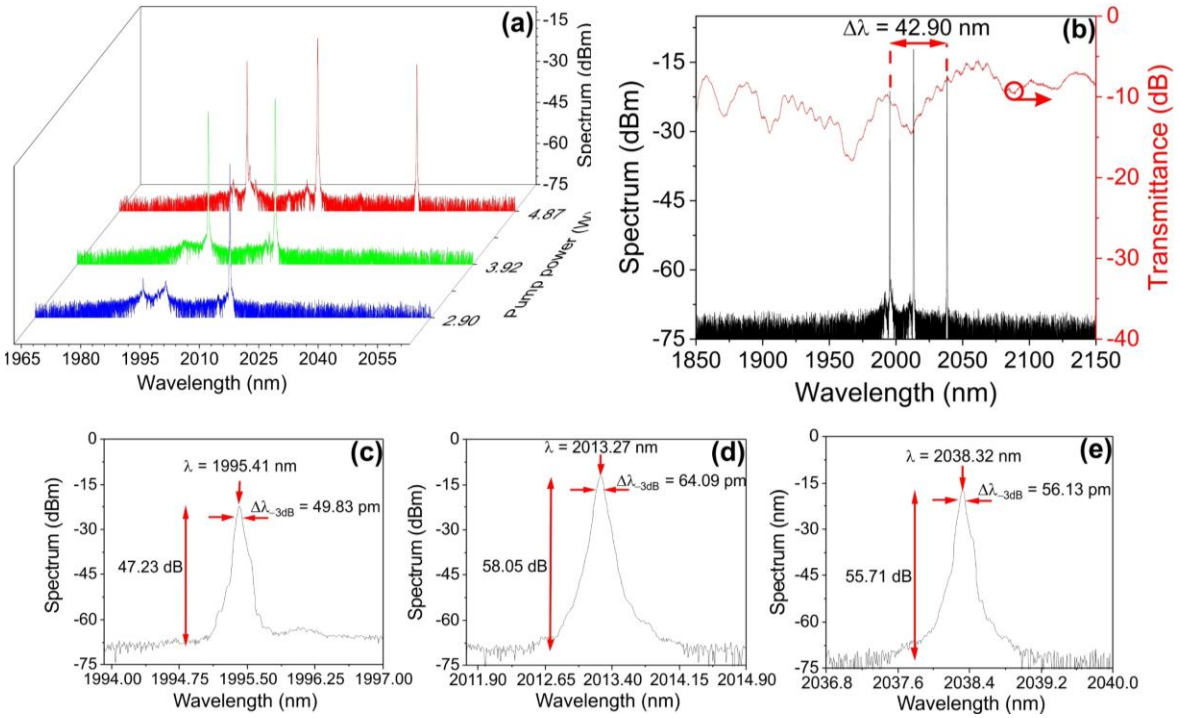


Fig. 7. Laser performance at simultaneous triple-wavelength operation as a function of pump power when applying 3.2 mm of linear displacement at the micrometric mount. (a) Spectral evolution as the pump power is increased between 2.90 and 4.87 W. (b) Detailed view of the triple-wavelength emission (black line) and MMI filter transmittance (red line) at 4.87 W pump power. Close-up view of laser linewidths corresponding to (c) 1995.41 nm, (d) 2013.27 nm and (e) 2038.32 nm.

The recorded stability for the lasing lines at 1995.41 nm (black line), 2038.32 nm (blue line) and 2013.27 nm (red line) are depicted in Fig. 8 over a total time span of 60 minutes. Fig. 8(a) illustrates the peak spectral power fluctuations, where variations of up to ±0.96, ±0.20 and ±3.45 dB were measured for the wavelengths of 1995.41 nm, 2013.27 nm and 2038.32 nm, respectively. These power fluctuations are significant due to several factors, such as strong mode competition, pump power fluctuations, vibrations of the mechanical elements, and room temperature variations. These effects alter the laser performance leading to peak spectral power variations of up to several decibels. However, laser stability could be improved by implementing active stabilization based on the electronic feedback from one of the cavity variables. In addition, Fig. 8(b) shows the variation in wavelength, this measurement reveals drifts of ± 33 pm, ± 8 pm and ± 35 pm for the 1995.41 nm, 2013.27 nm and 2038.32 nm wavelengths, respectively. These results demonstrate a high wavelength stability and reasonably good power uniformity for the proposed all-fiber laser scheme. The spectral evolution of the triple-wavelength emission is shown in the Fig. 8(c).

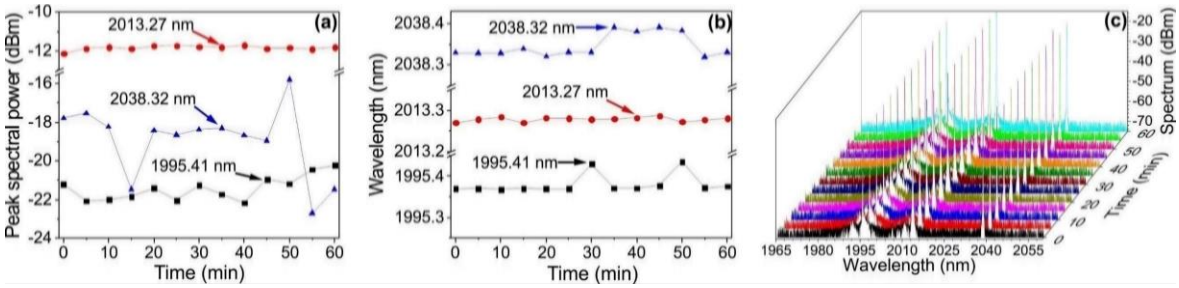


Fig. 8. Monitoring of the triple-wavelength emission with 4.87 W of pump power and 3.2 mm of mount displacement for the tapered MMI filter. (a) Peak spectral power fluctuation. (b) Wavelength variation. (c) The spectral evolution.

### *4.2.2 Switchable dual-wavelength performance with the tapered MMI filter*

After a slight adjustment of the PC and setting the pump power at 3.71 W, a dual-wavelength laser emission is obtained (black line), this mode of operation is observed when the tapered MMI filter is bent with 0.10 mm of mount displacement, as shown in Fig. 9(a), the red line trace depicted the MMI filter transmittance. The laser emission lines are centered at 1997.93 nm and 2032.15 nm with a Δλ of 34.27 nm. Variations in wavelength and output power were characterized over a time span of 60 minutes, as shown in Fig. 9(b). Whereas the lasing wavelengths do not display significant changes, peak spectral power variations of up to 3 dB are observed. The spectral evolution of the dual laser emission is depicted in Fig. 9(c). The emitted lines show narrow linewidths, the shorter wavelength reveals a 58.77 pm bandwidth with a SNR of 44.81 dB, whereas for the longer wavelength a −3 dB bandwidth of 56.87 pm is measured with a SNR of 52.08 dB. Close-up views of the generated laser lines are shown in Figs. 9(d) and (e).

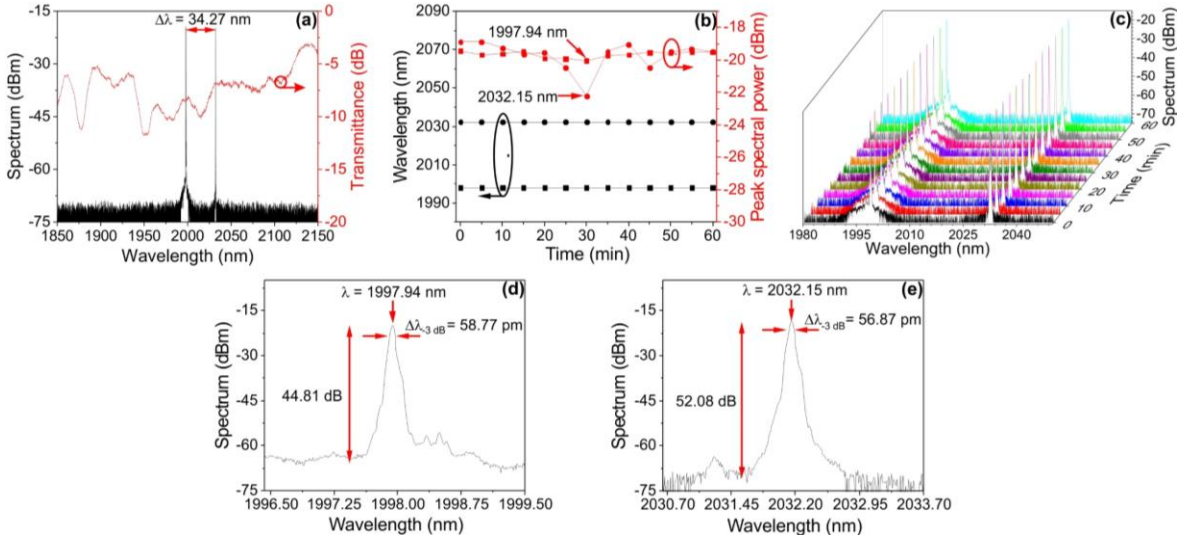


Fig. 9. (a) Dual-wavelength emission with 3.71 W pump power (black line) and output spectrum recorded at 0.10 mm of mount displacement for the tapered MMI filter (red line). (b) Monitoring of dual-wavelength emission variations (wavelength and peak spectral power). (c) Spectral evolution. Zoom-in of the generated laser linewidths corresponding to (c) 1997.94 nm and (d) 2032.15 nm.

The proposed scheme also allows switchable operation in dual-wavelength condition by controlling the polarization state into the cavity. Fig. 10(a) shows the switched laser line from dual to single operation at 2031.26 nm, where a peak spectral power of −16.31 dBm is observed. The efficiency was estimated to be around 0.41 %, as depicted in the inset. The stability in terms of the peak spectral power, output power and wavelength is shown in Fig. 10(b), where variations of up to ±0.59 dBm, ±0.12 mW and ±6 pm were measured over a time span of 60 minutes. Fig. 10(c) depicts the corresponding evolution of the single-wavelength emission at 2031.26 nm. Fig. 10(d) illustrates the switching behavior, suppressing the laser line at 2031.26 nm and emerging the laser emission centered around 1997 nm, where a peak spectral power of −19.09 dBm is observed. A close-up view of this laser emission reveals a close spacing (~ 0.6 nm) triple-wavelength generation at 1996.06 nm, 1996.50 nm and 1997.29 nm. The efficiency for these laser lines was around 0.35 %, as shown in the inset. The recorded variations in peak spectral power and wavelength are presented in Fig. 10(e), these were measured as ±0.33, ±2.91 and ±0.21 dBm and ±5, ±50 and ±5 pm for the set of wavelengths of 1996.06 nm, 1996.50 nm and 1997.29 nm, respectively. The corresponding spectral evolution for the triple-wavelength emission is shown in Fig. 10(f), where a zoom-in view to observe the laser lines is presented in the inset.

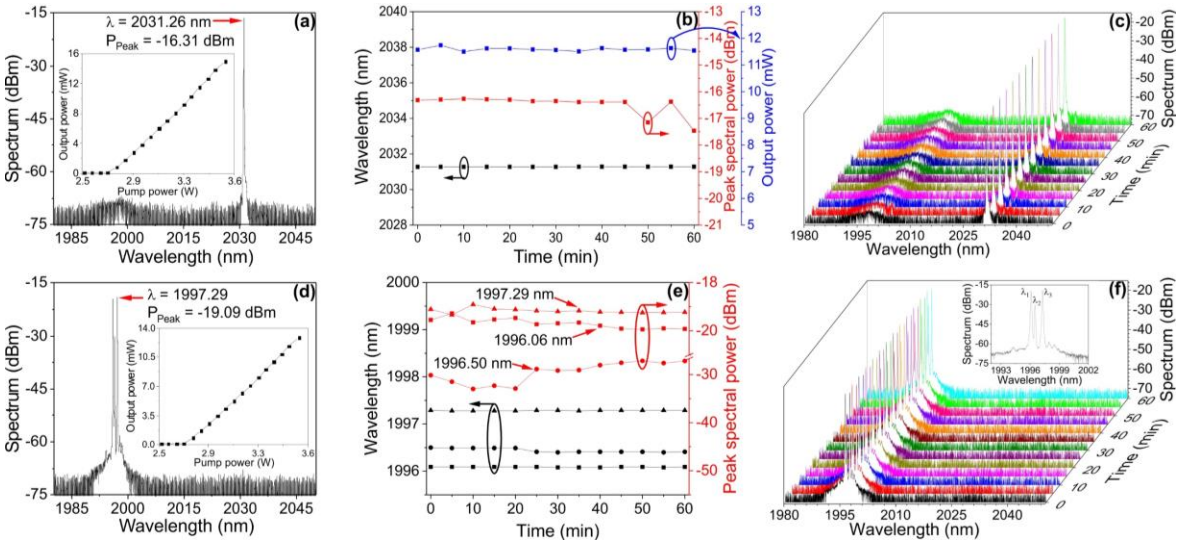


Fig. 10. Switching of dual-wavelength emission with 3.71 W of pump power and 0.10 mm of micrometric displacement. Single-wavelength operation at (a) 2031.26 nm and laser emission centered around (d) 1997.29 nm, where a triple-wavelength emission is observed. The inset includes the output power versus pump power. Laser stabilities recorded over a time span of 60 minutes for (b) 2031.26 nm and (e) the set of triple-wavelength emissions. Corresponding spectral evolution for (c) laser line at 2031.26 nm and (f) the set of laser emissions centered at 1997.29 nm, where a zoom-in view of the triple-wavelength emission is presented in the inset.

Compared to recently reported fiber lasers based on MMI structures [30-33], see Table 1. It is worth highlighting the capacity of the present scheme to provide a direct interaction with the surrounding medium, which is achieved via the coreless fiber, potentiating its performance as a sensor device. In addition, our approach improves the size of the MMI structure, reporting the minimum length of 18 mm by the inclusion of a tapered MMI filter. Beside these benefits, our proposal provides a tight control over the cavity parameters, enabling improvements on switching, single-, dual- or triple-wavelength emissions as a function of pump power, intracavity polarization state, and filter bending, making our laser system robust and functional. These experimental results, to the best of our knowledge, can be considered between the best results demonstrating multi-wavelength emission in the 2-μm band by using a fiber-based multi-mode interferometric device.

| Reference | Length of the MMI filter | Multimode Fiber Core | Multimode Fiber Cladding | Operation wavelength | Losses | Switching mechanism |
|---|---|---|---|---|---|---|
| **30** | 49.61 mm | NA | 125 μm | 1812.75 nm | 76% | Liquid concentration |
| | 48.07 mm | NA | | 1871.75 nm | 67% | |
| **31** | 50 mm | 105 μm | 125 μm | 2 μm | 6 dB | Pump power |
| | 200 mm | | | | | |
| **32** | 24 mm | 62.5 μm | 125 μm | 1900 nm | 8 dB | PC and strain |
| **33** | 127.1 mm | NA | 200 μm | 1812.74 nm | 4.44 dB | Liquid level |
| **This work - non tapered structure** | 43 mm | NA | 125 μm | 2 μm | 12.60 dB | Pump power, PC, bending |
| **This work - tapered structure** | 18 mm | NA | 125 μm | 2 μm | 8.74 dB | Pump power, PC, bending |

Table. 1. Comparison of the laser performance with recently reported fiber lasers based on MMI structures [30-33].

## 5. Conclusion

Stable multi-wavelength and switchable laser emission from a thulium-doped all-fiber laser based on two different types of MMI structures is demonstrated. The operation of the MMI filter relies on the induced curvature when applying a micrometric displacement on the linear translation stage mount. As a result of curvature, the MMI spectral response is blue shifted, allowing fine tuning of the filter response in the 2-micron wavelength region. The MMI operation is analyzed considering a tapered and non-tapered filter configurations, which in each case are composed of a SMF-COF-SMF arrangement. Using a non-tapered MMI filter, commutable dual-wavelength operation with a narrow bandwidth of ~50 pm, signal-to-noise ratio (SNR) over 50 dB, and maximum output power of 13.35 mW is achieved at 1986.34 nm and 2017.38 nm. For the tapered case, a minimum insertion loss of 8 dB is obtained in the 2-micron spectral band, and laser operation with single-, dual-, and triple-wavelength emissions are achieved with characteristics of narrow linewidth (50 pm) and high SNR (~60 dB) at the wavelengths of 1995.41 nm, 2013.27 nm and 2038.32 nm, respectively. A temporal analysis of the laser output reveals that pulsed light emission was not generated in our setup. Compared with similar reported TDFLs that include a MMI filter, our scheme is easily reproducible, preserves the simplicity and robustness of all-fiber arrangements and could be considered a reliable fiber-optic source that provides a high degree of repeatability.


## ACKNOWLEDGMENTS

This work was supported by CONACyT "Ciencia de Frontera 2019" under Grant 217560.


## References


[1] Michalska, M., Grzes, P., & Swiderski, J. (2018). 8.76 W mid-infrared supercontinuum generation in a thulium doped fiber amplifier. *Optical Fiber Technology*, *43*, 41-44, https://doi.org/10.1016/j.yofte.2018.04.003.

[2] Yang, L., Li, Y., Zhang, B., Wu, T., Zhao, Y., & Hou, J. (2019). 30-W supercontinuum generation based on ZBLAN fiber in an all-fiber configuration. *Photonics Research*, *7*(9), 1061-1065, https://doi.org/10.1364/PRJ.7.001061.

[3] Camarillo-Avilés, A., López-Estopier, R., Pottiez, O., Durán-Sánchez, M., Ibarra-Escamilla, B., & Bello-Jiménez, M. (2021). Supercontinuum source directly from noise-like pulse emission in a Tm-doped all-fiber laser with nonlinear polarization rotation. *Results in Optics*, *2*, 100040, https://doi.org/10.1016/j.rio.2020.100040.

[4] Jin, Q., Yin, T., Tu, Z., Chen, D., Shi, Y., Dai, D., & Gao, S. (2019). Performance evaluation of continuous-wave mid-infrared wavelength conversion in silicon waveguides. *Applied optics*, *58*(10), 2584-2588, https://doi.org/10.1364/AO.58.002584.

[5] Gunning, F. G., Kavanagh, N., Russell, E., Sheehan, R., O'Callaghan, J., & Corbett, B. (2018). Key enabling technologies for optical communications at 2000 nm. *Applied optics*, *57*(22), E64-E70, https://doi.org/10.1364/AO.57.000E64.

[6] Ghosh, A., Roy, A. S., Chowdhury, S. D., Sen, R., & Pal, A. (2016). All-fiber tunable ring laser source near 2 μm designed for CO2 sensing. *Sensors and Actuators B: Chemical*, *235*, 547-553, https://doi.org/10.1016/j.snb.2016.05.128.

[7] Sardar, M. R., Faisal, M., & Ahmed, K. (2021). Simple hollow Core photonic crystal Fiber for monitoring carbon dioxide gas with very high accuracy. *Sensing and Bio-Sensing Research*, *31*, 100401, https://doi.org/10.1016/j.sbsr.2021.100401.

[8] Fried, N. M. (2018). Recent advances in infrared laser lithotripsy. *Biomedical optics express*, *9*(9), 4552-4568, https://doi.org/10.1364/BOE.9.004552.

[9] Pal, D., Chowdhury, S. D., Dhar, A., Saraf, S., Maiti, K., Pal, D. K., ... & Pal, A. (2019). Ex vivo testing of air-cooled CW/modulated 30 W thulium fiber laser for lithotripsy. *Applied optics*, *58*(25), 6720-6724, https://doi.org/10.1364/AO.58.006720.

[10] Fried, N. M., & Irby, P. B. (2018). Advances in laser technology and fibre-optic delivery systems in lithotripsy. *Nature Reviews Urology*, *15*(9), 563-573, https://doi.org/10.1038/s41585-018-0035-8.
[11] Żywicka, B., Rybak, Z., Janeczek, M., Czerski, A., Bujok, J., Szymonowicz, M., & Świderski, J. (2020). Comparison of A 1940 nm thulium-doped fiber laser and A 1470 nm Diode laser for cutting efficacy and hemostasis in A pig model of spleen surgery. *Materials*, *13*(5), 1167, https://doi.org/10.3390/ma13051167.
[12] Shin, J. S., Cha, Y. H., Chun, B. J., Jeong, D. Y., & Park, H. (2021). 200-W Continuous-wave Thulium-doped All-fiber Laser at 2050 nm. *Current Optics and Photonics*, *5*(3), 306-310, https://doi.org/10.3807/COPP.2021.5.3.306.
[13] Michalska, M., Grześ, P., & Swiderski, J. (2019). High power, 100 W-class, thulium-doped all-fiber lasers. *Photonics Letters of Poland*, *11*(4), 109-111, https://doi.org/10.4302/plp.v11i4.953.
[14] Burns, M. D., Shardlow, P. C., Barua, P., Jefferson-Brain, T. L., Sahu, J. K., & Clarkson, W. A. (2019). 47 W continuous-wave 1726 nm thulium fiber laser core-pumped by an erbium fiber laser. *Optics letters*, *44*(21), 5230-5233, https://doi.org/10.1364/OL.44.005230.
[15] Ahmad, H., Samion, M. Z., Thambiratnam, K., & Yasin, M. (2019). Widely tunable dual-wavelength thulium-doped fiber laser operating in 1.8-2.0 mm region. *Optik*, *179*, 76-81, https://doi.org/10.1016/j.ijleo.2018.10.111.
[16] Escobar, E. H., Jiménez, M. B., Avilés, A. C., Estopier, R. L., Pottiez, O., Sánchez, M. D., & Andrés, M. V. (2019). Experimental study of an in-fiber acousto-optic tunable bandpass filter for single-and dual-wavelength operation in a thulium-doped fiber laser. *Optics express*, *27*(26), 38602-38613, https://doi.org/10.1364/OE.382166.
[17] Guo, Y., Yan, F., Feng, T., Qin, Q., Bai, Z., Li, T., ... & Suo, Y. (2022). Wavelength-interval-switchable multi-wavelength thulium-doped fiber laser with a nonlinear dual-pass Mach-Zehnder interferometer filter in 2-μm-band. *Optics & Laser Technology*, *145*, 107470, https://doi.org/10.1016/j.optlastec.2021.107470.
[18] Guo, Y., Yan, F., Feng, T., Qin, Q., Zhang, L., Guan, B., ... & Suo, Y. (2020). Stable multi-wavelength thulium-doped fiber laser with two cascaded single-mode-four-mode-single-mode fiber interferometers. *IEEE Access*, *9*, 1197-1204, https://doi.org/10.1109/ACCESS.2020.3044899.
[19] Soltanian, M. R. K., Ahmad, H., Khodaie, A., Amiri, I. S., Ismail, M. F., & Harun, S. W. (2015). A stable dual-wavelength Thulium-doped fiber laser at 1.9 μm using photonic crystal fiber. *Scientific reports*, *5*(1), 1-8, https://doi.org/10.1038/srep14537.
[20] Wang, M., Huang, Y., Yu, L., Song, Z., Liang, D., & Ruan, S. (2018). Multiwavelength thulium-doped fiber laser using a micro fiber-optic Fabry–Perot interferometer. *IEEE Photonics Journal*, *10*(4), 1-8, https://doi.org/10.1109/JPHOT.2018.2849998.
[21] Camarillo-Aviles, A., Jauregui-Vazquez, D., Estudillo-Ayala, J. M., Hernández-Escobar, E., Sierra-Hernández, J. M., Pottiez, O., & Bello-Jiménez, M. (2019). Stable multi-wavelength thulium-doped all-fiber laser incorporating a multi-cavity Fabry–Perot filter. *IEEE Photonics Journal*, *11*(6), 1-7, https://doi.org/10.1109/JPHOT.2019.2949500.
[22] Qin, Q., Yan, F., Liu, Y., Guo, Y., Li, T., Guan, B., & Feng, T. (2021). Stable, precisely controlled, and switchable thulium-doped fiber laser based on cascaded mode interference filters. *Optics Express*, *29*(7), 9786-9796, https://doi.org/10.1364/OE.419283.
[23] Qin, Q., Yan, F., Liu, Y., Zhang, L., Guo, Y., Han, W., & Zhou, H. (2021). Isolator-free unidirectional dual-wavelength thulium-doped fiber laser assisted by a two-mode fiber filter. *Optics & Laser Technology*, *134*, 106638, https://doi.org/10.1016/j.optlastec.2020.106638.
[24] Lau, K. Y., Abidin, N. Z., Cholan, N. A., Abas, A. F., Alresheedi, M. T., & Mahdi, M. A. (2019). Dual-wavelength thulium/holmium-doped fiber laser generation in 2 μm region with high side-mode suppression ratio. *Journal of Optics*, *21*(4), 045701, https://doi.org/10.1088/2040-8986/ab05af.
[25] Zhang, L., Yan, F., Feng, T., Guo, Y., Qin, Q., Zhou, H., & Suo, Y. (2019). Switchable multi-wavelength thulium-doped fiber laser employing a polarization-maintaining sampled fiber Bragg grating. *IEEE Access*, *7*, 155437-155445, https://doi.org/10.1109/ACCESS.2019.2944168.
[26] Theodosiou, A., Aubrecht, J., Kašík, I., Dousek, D., Komanec, M., & Kalli, K. (2021). Femtosecond Laser Plane-by-Plane Inscribed Cavity Mirrors for Monolithic Fiber Lasers in Thulium-Doped Fiber. *Sensors*, *21*(6), 1928, https://doi.org/10.3390/s21061928.

[27] Zhang, L., Yan, F., Feng, T., Han, W., Bai, Y., Bai, Z., ... & Suo, Y. (2019). Wavelength-tunable thulium-doped fiber laser with sampled fiber Bragg gratings. *Optics & Laser Technology*, *120*, 105707, https://doi.org/10.1016/j.optlastec.2019.105707.

[28] Durán-Sánchez, M., Álvarez-Tamayo, R. I., Posada-Ramírez, B., Ibarra-Escamilla, B., Kuzin, E. A., Cruz, J. L., & Andrés, M. V. (2017). Tunable dual-wavelength thulium-doped fiber laser based on FBGs and a Hi-Bi FOLM. *IEEE Photonics Technology Letters*, *29*(21), 1820-1823, https://doi.org/10.1109/LPT.2017.2752639.

[29] Guzman-Sepulveda, J. R., & Castillo-Guzman, A. A. (2021). Wavelength Tuning of Multimode Interference Fiber Lasers: A Review. *Advanced Photonics Research*, 2100051, https://doi.org/10.1002/adpr.202100051.

[30] Ibarra-Escamilla, B., Bravo-Huerta, E., Durán-Sánchez, M., Álvarez-Tamayo, R. I., Posada-Ramírez, B., Prieto-Cortés, P., ... & Kuzin, E. A. (2018). Dual-wavelength thulium-doped fiber laser with separate wavelengths selection based on a two mmi filters configuration. *Laser Physics*, *28*(9), 095107, https://doi.org/10.1088/1555-6611/aacb4f.

[31] Fu, S., Shi, G., Sheng, Q., Shi, W., Zhu, X., Yao, J., & Peyghambarian, N. (2016). Dual-wavelength fiber laser operating above 2 μm based on cascaded single-mode-multimode-single-mode fiber structures. *Optics express*, *24*(11), 11282-11289, https://doi.org/10.1364/OE.24.011282.

[32] Zhang, P., Wang, T., Ma, W., Dong, K., & Jiang, H. (2015). Tunable multiwavelength Tm-doped fiber laser based on the multimode interference effect. *Applied optics*, *54*(15), 4667-4671, https://doi.org/10.1364/AO.54.004667.

[33] Ma, X., Chen, D., Shi, Q., Feng, G., & Yang, J. (2014). Widely tunable thulium-doped fiber laser based on multimode interference with a large no-core fiber. *Journal of Lightwave Technology*, *32*(19), 3234-3238, 10.1109/JLT.2014.2342251.

[34] Soldano, L. B., & Pennings, E. C. (1995). Optical multi-mode interference devices based on self-imaging: principles and applications. Journal of lightwave technology, 13(4), 615-627, https://doi.org/10.1109/50.372474.

[35] Castillo-Guzman, A., Antonio-Lopez, J. E., Selvas-Aguilar, R., May-Arrioja, D. A., Estudillo-Ayala, J., & LiKamWa, P. (2010). Widely tunable erbium-doped fiber laser based on multimode interference effect. Optics express, 18(2), 591-597, https://doi.org/10.1364/OE.18.000591.

[36] Ma, W., Wang, T., Su, Y., Zhang, Y., Liu, P., Jia, Q., ... & Jiang, H. (2016). Wavelength-spacing switchable dual-wavelength single longitudinal mode thulium-doped fiber laser at 1.9 μm. *IEEE Photonics Journal*, *8*(6), 1-8, https://doi.org/10.1109/JPHOT.2016.2616515.

[37] Birks, T. A., & Li, Y. W. (1992). The shape of fiber tapers. *Journal of Lightwave Technology*, *10*(4), 432-438, https://doi.org/10.1109/50.134196.

[38] Ma, L., Qi, Y., Kang, Z., Bai, Y., & Jian, S. (2014). Tunable fiber laser based on the refractive index characteristic of MMI effects. *Optics & Laser Technology*, *57*, 96-99, https://doi.org/10.1016/j.optlastec.2013.10.001.